RIMS Kôkyûroku Bessatsu
B31 (2012), 79–92

Stable pattern selection through invasion fronts in closed two-species reaction-diffusion systems

By

Madeleine Kotzagiannidis, Jeremiah Peterson, Joseph Redford, Arnd Scheel, and Qiliang Wu

University of Minnesota, School of Mathematics, 206 Church St. S.E., Minneapolis, MN 55455, USA

Abstract

We study pattern formation in a two-species reaction-diffusion system with a conserved quantity. Such systems arise in the study of closed chemical reactors and recurrent precipitation. We compare pattern forming aspects in these systems to Turing-pattern forming systems. We show that in a zero-diffusion limit, these systems possess stable periodic patterns. We also exhibit a wavenumber-selection mechanism in this limit: While spatially random initial conditions give patterns on arbitrarily fine scales, localized initial conditions evolve into a coherent pattern with a finite wavenumber that is formed in the wake of invasion fronts. We compare our theoretical results with numerical simulations and point to an interesting front instability in a small mass fraction regime.

§ 1. Introduction

Turing [18] predicted that the coupling of reaction and diffusion can lead to pattern-forming instabilities. The effect in its simplest form can be observed in linear reaction-diffusion systems with two species, posed on the real line. Key ingredient is a disparity in the mobility of the two species. Only much later, such patterns were actually realized experimentally [1, 4]. The experimental setup involved an open-flow reactor: the system is not in equilibrium and patterns are sustained through a continuous supply of reactants.

Some 50 years earlier, Liesegang [9] had observed pattern-forming processes in a simple reaction-diffusion setup. The patterns he observed were created in a gel, very much like the patterns in the experimental setup in [4], both according to Turing's assumption that diffusion alone would suffice to create patterns. The reaction process in Liesegang's systems was significantly simpler, involving a reaction between two electrolytes and a precipitation process. Pattern formation in this context is attributed to the precipitation process which is often modeled by a nonlinear reaction-diffusion system for precipitate and solute, with a conversion rate that reflects saturation and super-saturation thresholds. We study such a model in more detail in this paper.

Supersaturation models for precipitation processes are similar to models for Turing pattern formation but exhibit some key differences. Our goal here is to elucidate these parallels and differences and point to a number of interesting phenomena associated with wavenumber selection in precipitation models.

Received June 30, 2011.
2000 Mathematics Subject Classification(s): 92E20

At first glance, one notices that Liesegang patterns are *not* periodic, but the wavenumber decreases as distances between precipitation bands increase in a geometric sequence. On the other hand, Liesegang patterns are created in a closed system: an outer electrolyte is inserted into the system only at an initial time. Also, Liesegang patterns are created in the wake of a moving front, triggered by the diffusion of the outer electrolyte into the gel. We showed in [7, 8] how *periodic* patterns are created in the wake of a uniformly and rigidly translating front. Precipitation systems and Turing systems share a key feature, the difference in diffusion constants for the two species: similar to Turing's mechanism, precipitation models always include slow diffusion for one species (the precipitate) compared to the other (the solute).

Our focus here will be on a model for precipitation with a simple cubic nonlinearity, which has been studied in [7, 8] in connection with Liesegang patterns and wavenumber selection. We denote by c the concentration of the solute and by e the concentration of the precipitate, and consider the one-dimensional caricature of a precipitation system

$$\begin{aligned} c_t &= c_{xx} - e(1-e)(e-a) - \gamma c \\ e_t &= \kappa e_{xx} + e(1-e)(e-a) + \gamma c. \end{aligned} \tag{1.1}$$

Here, $\gamma > 0$ and $a \in (0,1)$ are parameters, and $x \in \mathbb{R}$ is the idealized spatial domain. The diffusion constant κ of the precipitate will be assumed to be small, $0 \leqslant \kappa < 1$. Shifting e and c one can easily arrange for the positive quadrant $c, e \geqslant 0$ to be forward invariant, with cubic $-e(e-a)^2$, but the form (1.1) will be slightly more convenient for us.

Note that (1.1) is also a prototype for a simple *closed* reaction-diffusion system, with conserved quantity $m = c + e$. In the remainder of this article, we analyze wavenumber selection in this system, with focus on the case $\kappa = 0$. We sometimes write $f(c, e) = e(1-e)(e-a) + \gamma c$.

Acknowledgments. The authors gratefully acknowledge support through NSF grants DMS-0806614 and DMS-1138495.

§ 2. Temporal wavenumber selection

Linearizing at an equilibrium $c = 0, e = a$, and using Fourier transform, we find the family of linear equations

$$\begin{aligned} c_t &= -k^2 c - f_e e - f_c c \\ e_t &= -\kappa k^2 e + f_e e + f_c c. \end{aligned} \tag{2.1}$$

Here, $f_e = a(1-a) > 0$ and $f_c = \gamma > 0$. This system is unstable when $f_e > \kappa f_c$. The fastest growing solution to this family of equations has wavenumber k_{temp}, and all wavenumbers with $|k| \leqslant k_{\max}$ are (marginally) unstable, where

$$k_{\text{temp}} = \sqrt{\frac{-\kappa(f_c + f_e) + \sqrt{\kappa(1+\kappa)^2 f_c f_e}}{\kappa(1-\kappa)}}, \qquad k_{\max} = \sqrt{\frac{f_e - \kappa f_c}{\kappa}}. \tag{2.2}$$

We emphasize that both, k_{temp} and $k_{\max}$ diverge to ∞ when $\kappa \to 0$. Also, for $\kappa > 0$, k_{temp} and $k_{\max}$ are $\mathrm{O}(\varepsilon)$ near onset of instability, that is, when $f_e = \kappa f_c + \varepsilon^2$.

Beyond those linear predictions, one can also investigate existence of nonlinear patterns with a prescribed spatial wavenumber. Adding the equations $c_t = e_t = 0$, integrating, and introducing $\mu \equiv c + \kappa e$, we obtain

$$\kappa e_{xx} + e(1-e)(e-a) + \gamma(\mu - \kappa e) = 0.$$

One finds families of even periodic solutions parameterized by μ and wavenumber k for fixed γ, a. All those patterns are, however, unstable when considered as solutions on the real line — they are in fact unstable with respect to perturbations of twice their minimal period [7, 11, 12, 13].

One can compare these findings with typical situations in Turing pattern forming systems, such as the Gray-Scott model, the Brusselator, Gierer-Meinhardt systems, or, most simply, the Swift-Hohenberg equation. These systems possess an equilibrium state that destabilizes as a parameter is varied in what is referred to as a Turing instability. Close to instability, there exists a band of unstable wavenumbers $k_- < k < k_+$, with $0 < k_\pm < \infty$. There also exist nonlinear stable spatially periodic (Turing) patterns for a range of spatial periods.

Closed reaction-diffusion that we consider here are similar to Turing-pattern forming systems in that

- they exhibit linear wavenumber selection, that is, fastest growing linear modes with nonzero wavenumber, and
- they possess nonlinear periodic patterns for a range of wavenumbers.

They are different from Turing systems since

- periodic patterns are all unstable, and
- there is no Turing instability, with finite selected wavenumber at onset.

The remainder of this paper therefore focuses on the limiting case where $\kappa = 0$. We will first consider existence and stability of stationary patterns in this system on L^∞-spaces.

Lemma 2.1. Consider (1.1) with $\kappa = 0$ on $L^\infty(\mathbb{R})$. The equation generates a smooth local semiflow on $X = L^\infty(\mathbb{R}) \times L^\infty(\mathbb{R})$ and possesses a family of equilibria with $c(x) \equiv 0$ and $e(x) \in \{0, a, 1\}$, so that $e^{-1}(a)$ and $e^{-1}(1)$ are measurable. In the case when $e(x) \in \{0, 1\}$, those patterns are asymptotically stable. More precisely, any solution with initial condition L^∞-close to such an equilibrium will converge to the equilibrium exponentially in L^∞ as $t \to \infty$.

Proof. The unbounded operator $(c, e) \mapsto (c_{xx} - \gamma c, 0)$ is sectorial (although not densely defined [10]) on X and the nonlinearity $e \mapsto e(1 - e)(e - a)$ is smooth as a superposition operator on $L^\infty(\mathbb{R})$, which together gives local existence and smooth dependence on initial conditions. Functions with $c \equiv 0$ and $e \in \{0, a, 1\}$ are clearly equilibria, so that it remains to conclude asymptotic stability. This in turn can be readily concluded once we establish that the spectrum of the linearization is contained in $\operatorname{Re}\lambda \leqslant -\delta < 0$. To see this, consider the linearized operator

$$\mathcal{L}\begin{pmatrix} c \\ e \end{pmatrix} := \begin{pmatrix} -\partial_{xx} - \gamma & -g'(e_*(x)) \\ \gamma & g'(e_*(x)) \end{pmatrix} \begin{pmatrix} c \\ e \end{pmatrix},$$

where $g(e) = e(1 - e)(e - a)$. When $e_*(x) \neq a$ almost everywhere, then $g'(e_*(x)) < -\delta < 0$. As a consequence, one finds through a short explicit calculation that $\mathcal{L} - \lambda$ is bounded invertible for all λ with $\operatorname{Re}\lambda \geqslant 0$, which guarantees linear asymptotic stability as claimed. Nonlinear stability follows immediately from a variation-of-constants argument. ∎

With this result we can contrast the case $\kappa = 0$ with the case $\kappa > 0$ and Turing-pattern forming systems.

	Turing	Precipitation $\kappa > 0$	Precipitation $\kappa = 0$
linear wavenumber selection	$0 < k_{\text{temp}} < \infty$	$0 < k_{\text{temp}} < \infty$	$k_{\text{temp}} = \infty$
nonlinear patterns	periodic	periodic	periodic & aperiodic
nonlinear patterns stable	yes	no	yes
Turing bifurcation	yes	no	no

In other words, the case $\kappa = 0$ supports stable periodic patterns, but does not exhibit a mechanism for wavenumber selection, neither linearly through the dispersion relation, nor nonlinearly.

The simulations in Figure 2.1 show how the presence of small diffusion in the precipitate selects a band of dominant wavenumber in the systems, which then evolves through a coarsening process, reflecting the instability of periodic patterns. We simulated (1.1) with initial conditions given as a small perturbation of $c = 0, e = a$ in both c- and e-component. We constructed the perturbation using $3k_{\max}$ Fourier modes with amplitudes chosen from a uniform random distribution in $[0, 0.1]$. Here, $k_{\max}$ is chosen from (2.2) using $\kappa = 0.2$, $f_e = a(1-a)$, and $f_c = \gamma$. In the absence of diffusion, $\kappa = 0$, stationary patterns are created from random initial conditions, however without an apparent selected wavenumber.

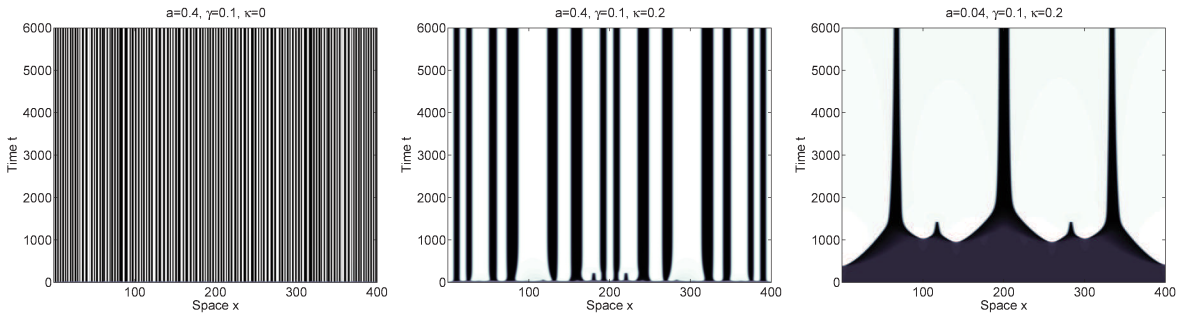

Figure 2.1: Simulations with Fourier randomized initial perturbations (see text for details) of $c = 0, e = a$. The pictures show gray-scale space-time plots, where $e = 0$ corresponds to black and $e = 1$ to white. The left picture shows $a = 0.4$, with zero diffusion $\kappa = 0$. The middle picture shows $a = 0.4$, with small diffusion $\kappa = 0.2$. The right picture shows a smaller a-value $a = 0.04$ with diffusion $\kappa = 0.2$. Throughout, $\gamma = 0.1$.

§ 3. Spatial wavenumber selection

A slightly different class of randomized initial conditions leads to dramatically different resulting patterns. When one forces initial perturbations of an unstable state to be spatially localized, the solution involves into a pair of *coherent* invasion fronts, leaving behind a regular periodic pattern with a distinguished wavelength. Figure 3.1 contrasts localized and uniformly random initial conditions and illustrates the corresponding crossover. We chose initial conditions as perturbations of the spatially homogeneous, unstable state $(c, e) = (0, a)$. We chose the perturbations as piecewise constant on intervals of length 3, with values in $\{-\delta, 0, \delta\}$, $\delta = 0.1$, with probabilities $\{\alpha, 1-2\alpha, \alpha\}$. For small α, perturbations are localized in space with expected value for the distance $3 \cdot \frac{1}{2\alpha}$. For $\alpha \sim 0.5$, perturbations are non-local. One expects a crossover between correlated patterns and random patterns for spacings $3/2\alpha \sim 2\pi/k$, where k is the wavenumber in the wake of invasion fronts. Using the predicted values for $k = k_{\text{lin}}$ derived below, this corresponds to $\alpha \sim 0.085$. Figure 3.1 shows the resulting increase in coherence of patterns for $\alpha = 0.015, 0.09, 0.33$.

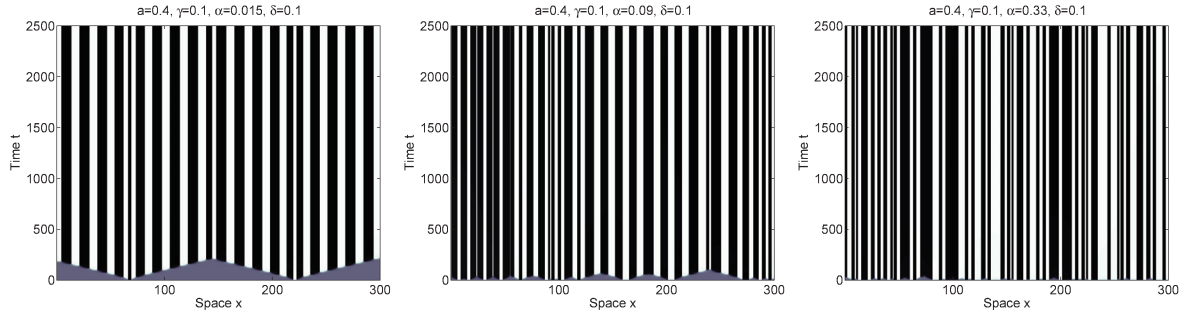

Figure 3.1: Simulations with white noise random initial perturbations (see text for details) of $c = 0, e = a$. The pictures show gray-scale space-time plots, where $e = 0$ corresponds to black and $e = 1$ to white. Parameters are $a = 0.4$, $\gamma = 0.1$, and zero diffusion $\kappa = 0$. Nucleation events appear with probability $\alpha = 0.015$, 0.09, 0.33 and amplitude $\delta = 0.1$ from left to right.

In the following, we derive a linear criterion that predicts the selected wavenumber in the wake of an invasion front; see [19] for a review of front propagation into unstable states. We look for solutions to the linearized equation in a comoving frame $\xi = x - st$ via the ansatz $(c, e) = (c_0, e_0)\mathrm{e}^{\lambda t+\nu\xi}$. Nontrivial solutions exist when the complex dispersion relation $d_s(\lambda, \nu)$ vanishes, where

$$d_s(\lambda, \nu) = d(\lambda - s\nu), \qquad d(\lambda, \nu) = \lambda^2 - (f_e - f_c + (1 + \kappa)\nu^2)\lambda - (\kappa f_c - f_e)\nu^2 + \kappa\nu^4.$$

We say solutions to (2.1) with compactly supported initial condition decay pointwise in a comoving frame $\xi = x - st$ if they decay for fixed ξ. We then define the linear spreading speed as the supremum of all speeds s so that there are compactly supported initial conditions that do not decay pointwise.

It is well known that pointwise decay is equivalent to the absence of *pointwise growth modes* in the unstable half plane $\operatorname{Re}\lambda > 0$; see [3, 2, 5, 6, 14, 16]. These pointwise growth modes correspond to double roots of d_s that satisfy the pinching condition:

$$d_s(\lambda, \nu) = 0, \quad \partial_\nu d_s(\lambda, \nu) = 0, \quad \operatorname{Re}\nu_\pm(\lambda) \to \pm\infty \text{ for } \lambda \to \infty,$$

where the $\nu_\pm(\lambda)$ are the continuations of the two roots ν of $d_s(\lambda, \nu)$ that collide in the double root, and λ follows a curve where $\operatorname{Re}\lambda$ increases monotonically to $+\infty$.

As a consequence, we will see that the linear spreading speed is the largest value s so that

$$d_s(\mathrm{i}\omega, \nu) = 0, \quad \partial_\nu d_s(\mathrm{i}\omega, \nu) = 0, \quad \operatorname{Re}\nu_\pm(\lambda) \to \pm\infty \text{ for } \lambda \to \infty.$$

Associated with this specific value of $s = s_{\mathrm{lin}}$ is the marginally stable pointwise growth mode $\lambda = \mathrm{i}\omega_{\mathrm{lin}}$ and a complex spatial decay rate ν. An oscillation of frequency ω in a moving frame of speed s creates a spatial pattern of wavenumber $k = \omega/s$. We refer to this wavenumber $k = k_{\mathrm{lin}}$ as the *spatially selected wavenumber*.

Lemma 3.1. Suppose $\kappa = 0$ and $f_c, f_e > 0$, $f_c > \kappa f_e$. Then the spatially selected wavenumber is nonzero, that is, $s_{\mathrm{lin}} > 0$, $\omega_{\mathrm{lin}} \neq 0$ and $k_{\mathrm{lin}} \neq 0$.

We prove the lemma in the appendix.

Corollary 4.15 in [8] shows that the existence of invasion fronts of the form $(c, e)(x - st, \omega t)$ that converge to $(c, e) = (0, a)$ for $x \to +\infty$ with exponential rate at least $\operatorname{Re}\nu$ and to $(c, e)(kx)$, $k = \omega/s$

is a robust phenomenon — without showing actual existence. Existence can sometimes be shown using topological arguments, as exemplified in the case of the Cahn-Hilliard equation; see [17].

In order to compute linear spreading speeds numerically, one needs to find the largest value of s so that there is a double root (λ, ν) with $\operatorname{Re}\lambda = 0$. One can directly compute such roots numerically and then continue in the parameter γ. In order to show that the curve of spreading speeds computed in this fashion gives the supremum, one needs to establish that there are no pinched double roots on the imaginary axis for larger values of s. In our case, this can be verified by continuing the complex double root in s to large values of s due to Lemma 7.7, which guarantees that there is at most one complex double root. Summarizing, one can determine spreading speeds by continuing the complex double root in s, decreasing s until $\operatorname{Re}\lambda = 0$. We found numerically that $\operatorname{Re}\lambda$ is monotone in s, so that the speed as a solution of $d_s(\mathrm{i}\omega, \nu) = 0$, $\partial_\nu(\mathrm{i}\omega, \nu) = 0$ is in fact unique. We were however not able to prove this fact analytically. The results are plotted in Figures 4.1 and 4.2, together with data from direct simulations.

§ 4. Numerical experiments versus linear prediction

In the following, we compare the linear predictions with numerical simulations. We solve (1.1) on a domain $x \in [0, L]$, $L = 700$, with Neumann boundary conditions, using second-order finite differences ($\delta x = 0.1$) and implicit Euler time stepping ($\delta t = 0.05$). Results are robust to grid refinements. We start with initial condition $(c, e) = (0, a) + (\delta c(x), 0)$, where a is a parameter and $\delta c(x)$ has support on $x \in [0, 20]$. Figure 4.1 shows a sequence of space-time plots for $\gamma = 0.1$, Figure 4.2 shows the corresponding results for $\gamma = 1.5$.

Wavenumbers and speeds in the direct simulations compare well to wavenumbers and speeds predicted by the linear dispersion relation as illustrated in Figure 4.3. The most significant difference between linear predictions and direct simulations occurs for small values of a.

Figure 4.4 illustrates the transition near a_* in some more detail. One notices that the wavenumber in the wake oscillates since some nucleation events in the leading edge of the front do not pass a threshold and eventually do not create a spike. We found that the average effective wavenumber in the wake drops by roughly a factor 2/3. Note that the transition is intermittent, so that wavenumber averages are inherently unreliable. A somewhat simplistic view would characterize this transition in a comoving frame as a Hopf bifurcation from the primary invasion front. Since the primary front is a periodic orbit in a comoving frame one expects frequency locking for the bifurcating fronts, a prediction that is consistent with the observed strong resonance in frequencies $\omega/\omega_{\mathrm{lin}} \sim 2/3$. We note that this simple view does not explain the apparent intermittent nature of the bifurcation.

Similar transitions have been observed in [8] for non-vanishing diffusion $\kappa = 0.1$; see Figure 14, there. On the other hand, robustness arguments based on counting of Morse indices in [8] indicate that for small γ, pattern-forming fronts are typically not robust. The reason is that periodic patterns are unstable for small γ with respect to perturbations of the *same* (minimal) period. This leads to a resonance between the instability and the invasion process that effectually destroys the pattern in the wake of the front after a short transient; see again [8, Fig. 8,9,11 and Thm 1.2]. We notice however that for $\kappa = 0$, periodic patterns in the wake are stable regardless of the value of γ!

One might also be tempted to compare these findings with observations in the Cahn-Hilliard equation. There, invasion fronts also leave behind a pattern which is unstable. The instability in the wake of the pattern leads to a secondary invasion front that follows the primary front. One can (numerically) compute invasion speeds for this secondary front and finds that for small mass fractions, the secondary front is in

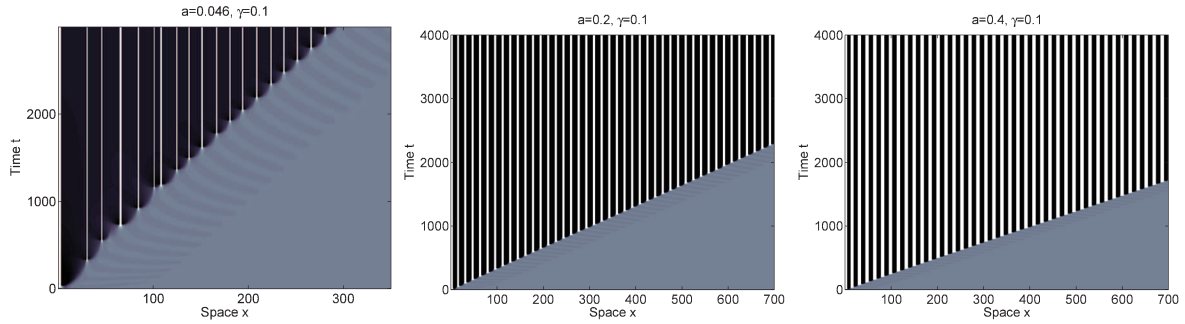

Figure 4.1: Gray-scale space-time plots of $e(t,x)$ ($e=0$ black, $e=1$ white) for varying $a=0.046, 0.2, 0.4$ and $\gamma=0.1$. One notices a drop in wavenumber when precursors fail to nucleate spikes. For most parameter values, the pattern in the wake is not periodic but intermittent.

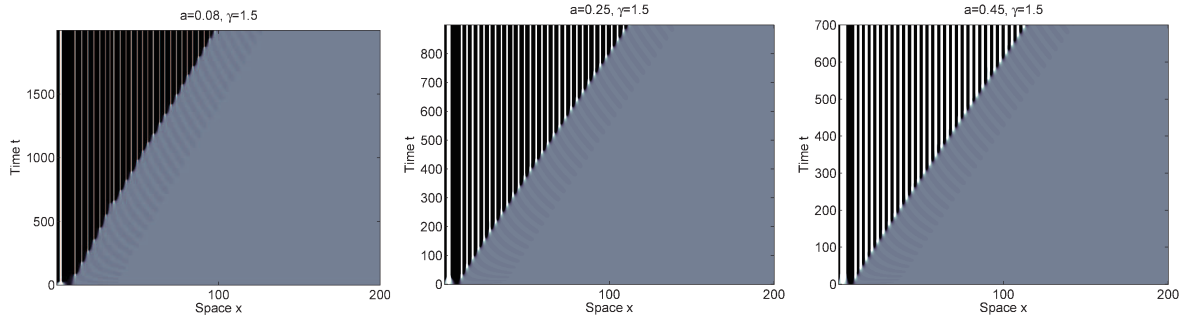

Figure 4.2: Space-time plots of $e(t,x)$ ($e=0$ black, $e=1$ white) for varying $a=0.08, 0.25, 0.45$ and $\gamma=1.5$. Similar to the case of γ small, one notices a drop in wavenumber for small a.

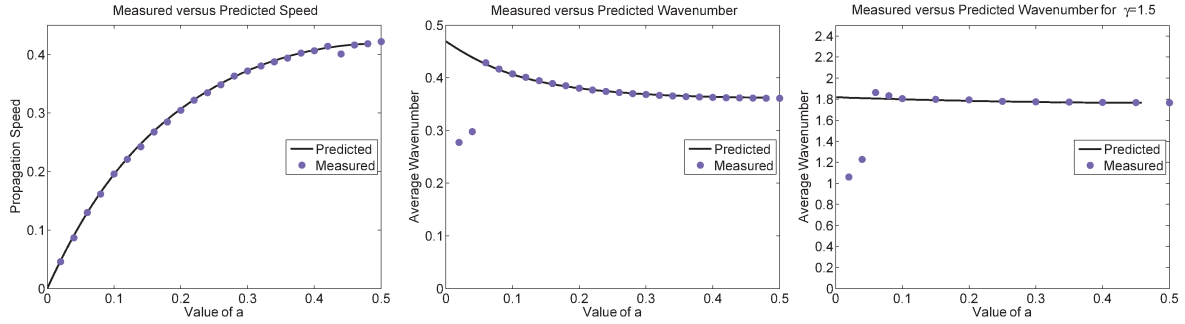

Figure 4.3: Wavenumbers and speeds as functions of a in direct simulations compared to the predictions from the dispersion relation. The left figure shows good agreement of s for all values of a, fixing $\gamma=0.1$. The middle and right figure show agreement of k for values of a larger than $a_* \sim 0.05$, for $\gamma=0.1$ (middle) and $\gamma=1.5$ (right).

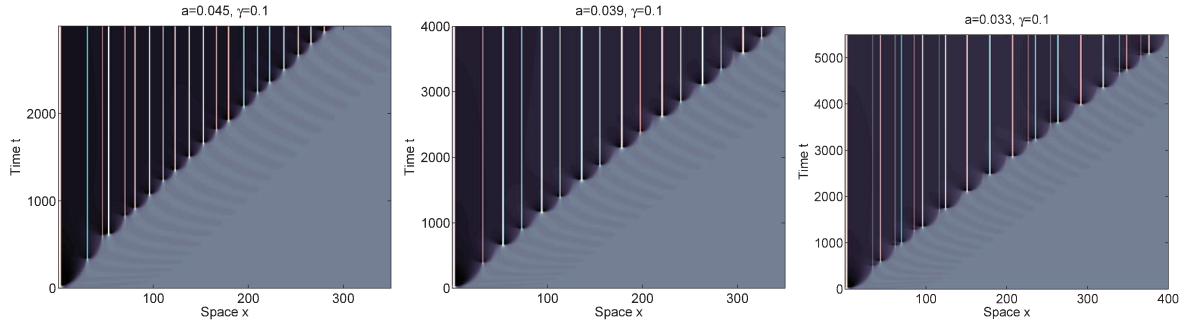

Figure 4.4: Space-time plots of solutions $e(t,x)$ ($e = 0$ black, $e = 1$ white) for small values of $a = 0.045, 0.039, 0.033$. One notices the intermittent nature of the drop in wavenumbers.

fact faster than the primary front. As a result, one does not see the predicted wavenumber in the wake of the front but an 'instantaneously coarsened', smaller wavenumber. Comparison with direct simulations indicate that the secondary front already locks with the first front for parameter values when its predicted speed is slower than the speed of the primary front. We envision that this locking can be explained by a front instability caused by point spectrum rather than an absolute instability in the wake of the front; see [15] for a similar phenomenon. In the case $\kappa = 0$, the patterns in the wake are stable, so that point spectrum would necessarily cause the observed instability.

§ 5. Bulk fronts

Up to now, we have investigated how localized initial perturbations evolve into a pattern-forming front. When gradually relaxing the assumption of localization, one encounters an interesting crossover from pattern-forming to bulk fronts, that is, fronts that leave behind a spatially homogeneous state. In the following, we investigate this phenomenon and compare our theoretical predictions with direct simulations.

We envision perturbations of the initial unstable state $(c,e)(x) = (0,a)$ by a small, exponential profile $c(x) = \delta e^{\nu|x|}$. For $0 > \operatorname{Re}\nu > \operatorname{Re}\nu_{\mathrm{lin}}$, that is, when the decay of the initial condition is weaker than the decay of the selected pointwise growth mode, one observes fronts with different speeds s and frequency ω. Given ν, one can predict ω and s by solving the dispersion relation

$$d_s(\mathrm{i}\omega,\nu) = (\mathrm{i}\omega - s\nu)^2 - (1-2\gamma+\nu^2)(\mathrm{i}\omega - s\nu) + (1-\gamma)\nu^2,$$

for s and ω (we normalized $f_e + f_c = 1$). In fact, $\operatorname{Im} d_s(\mathrm{i}\omega,\nu) = 0$ leads to either $\omega = 0$ or $s = -\frac{\nu^2-(1-2\gamma)}{2\nu}$, when $\operatorname{Im}\nu = 0$, that is, for monotone exponential tails in the initial conditions. The case $\omega = 0$ leads to a quadratic equation in s, which possesses real roots only when

$$|\nu| \leqslant \eta_{\mathrm{crit}} := |\sqrt{1-\gamma} - \sqrt{\gamma}|. \tag{5.1}$$

One finds roots with $\omega \neq 0$ in the case when (5.1) does not hold, by substituting $s = -\frac{\nu^2-(1-2\gamma)}{2\gamma}$ and solving for ω. As a consequence, we predict a transition from pattern-forming fronts to uniformly translating fronts at $|\nu| = \eta_{\mathrm{crit}}$.

We compared this prediction with simulations, where $a = 0.5$, hence $f_e = 0.25$, and $f_c = 0.1$. Scaling to $f_e + f_c = 1$ gives a critical value of $\eta_{\mathrm{crit}} = 0.184$. Figure 5.1 shows space-time plots close to the transition.

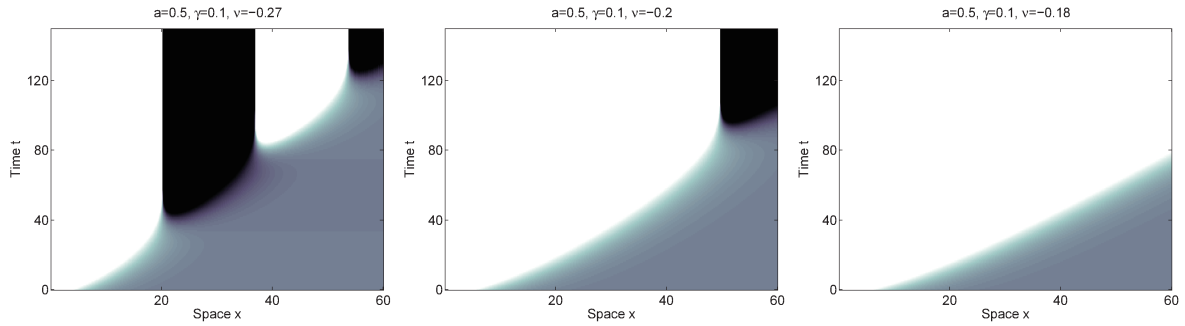

Figure 5.1: Space-time plots of solutions $e(t,x)$ ($e=0$ black, $e=1$ white) for initial perturbations with decay $\mathrm{e}^{\nu x}$, with $\nu=-0.27,-0.2,-0.18$. Throughout, $a=0.5$ and $\gamma=0.1$.

One can also compute selected wavenumbers for ν complex. In this case, we typically find $\omega\neq 0$. For small $|\operatorname{Re}\nu|$, one finds that $k\sim\operatorname{Im}\nu$: the wavelength of the initial condition translates directly into the wavelength of the spatial pattern. For small $|\operatorname{Im}\nu|$, one finds a crossover near $\operatorname{Re}\nu=-\eta_{\mathrm{crit}}$, where the wavelengths in the wake change from $|\operatorname{Im}\nu|$ to an intrinsic wavelength selected by the system.

We emphasize that this transition is different from a transition from pattern-forming to bulk fronts that was observed in [8]. There, we observed that for small values of a and γ, front invasion leaves behind a bulk state. In this regime, fronts are "pushed" [19], that is, steeper and faster than predicted by the linear dispersion relation. The regime of pushed front propagation is limited by $a\leqslant a_*(\kappa)$ and $a_*(\kappa)\to 0$ for $\kappa\to 0$ for small γ.

§ 6. Discussion

We presented a simple and robust mechanism for the creation of stable periodic patterns in a closed, two-species reaction-diffusion system. Since smooth periodic patterns are unstable in closed, two-species systems, we investigated the limit of vanishing diffusion. In this sharp-interface limit, the sideband instability of periodic patterns disappears. On the other hand, linear growth rates in the dispersion relation predict patterns on infinitely fine scales, a prediction that is corroborated in simulations with white noise initial data. Stable periodic patterns with a distinguished wavelength are, however, selected when initial conditions are spatially localized. Instabilities evolve through pattern-forming invasion fronts that leave behind a coherent pattern — even in the case of zero diffusion. We showed rigorously that the linear prediction for the selected wavenumber is finite for zero diffusion.

An interesting phenomenon arises for small mass fractions, when linear predictions for wavenumbers disagree with direct simulations. Phenomenologically, one observes that small modulations in the leading edge of the invasion front repeatedly fail to nucleate spikes. The resulting pattern is typically quasi-periodic with average wavenumber about 2/3 of the linear prediction close to transition. It would be interesting to characterize this transition conceptually and predict the intermittent behavior of spiking at least qualitatively.

§ 7. Appendix

§ 7.1. Proof of Lemma 3.1

Our goal is to prove that the supremum in the definition of the spreading speed is actually attained when a double root that satisfies the pinching condition is located on the imaginary axis, $\lambda \in \mathrm{i}\mathbb{R} \setminus \{0\}$. We outline the general strategy of proof.

We first show that double roots of the dispersion relation (disregarding the pinching condition for now) are continuous with respect to s in Lemma 7.1. We then show that the real part of the pointwise growth rate is continuous in s, showing some type of continuity for the pinching condition; see Lemma 7.3.

Given continuity, we then show existence of a critical double root $\lambda = \mathrm{i}\omega$ using that pointwise growth rates are negative for $s \gg 1$, Lemma 7.4, and positive for $s \sim 0$, Lemma 7.5. Lastly, we exclude the case $\omega = 0$ for a double root by a direct calculation, Lemma 7.6.

Lemma 7.1. Double roots (ν, λ) of the dispersion relation vary continuously with respect to s.

Proof. By a straightforward computation, the double root equation

$$d_s(\lambda, \nu) = 0, \quad \partial_\nu d_s(\lambda, \nu) = 0$$

can be rewritten as

- for $s \neq 1$,

$$\begin{cases} -2s\nu^5 - s^2\nu^4 + 4s\nu^3 + [4\gamma(1-\gamma) + 2s^2]\nu^2 - 2(1-2\gamma)^2 s\nu - (1-2\gamma)^2 s^2 = 0 \\ \lambda = s\nu + \frac{s(1-2\gamma+\nu^2)+2(1-\gamma)\nu}{2(s+\nu)} \end{cases} \tag{7.1}$$

- for $s = 1$, $\nu = -1$,

$$(\nu, \lambda) = (-1, -\gamma \pm \sqrt{(1-\gamma)^2 - (1-\gamma)})$$

- for $s = 1$, $\nu \neq -1$,

$$\begin{cases} (\nu + 1 - 2\gamma)^2 - 2(1 - 2\gamma + \nu^2)(\nu + 1 - 2\gamma) + 4(1-\gamma)\nu^2 = 0 \\ \lambda = s\nu + \frac{s(1-2\gamma+\nu^2)+2(1-\gamma)\nu}{2(s+\nu)} \end{cases}$$

We first note that there are precisely 5 double roots (counted with multiplicity) when $s \neq 1$, since the first equation in (7.1) is a quintic polynomial. As solutions to a polynomial equation, these double roots depend continuously on s. Next, note that roots obtained in the case for $s = 1$ agree with those obtained in the case $s \neq 1$ when formally setting $s = 1$ in the quintic polynomial for ν. Therefore, to prove the continuity, we only need to show that for $s \to 1$, $s \neq 1$, there are two double roots (λ_1, ν_1) and (λ_2, ν_2) such that

$$\begin{aligned} \lim_{s\to 1} \lambda_1 &= -1, \quad \lim_{s\to 1} \nu_1 = -\gamma + \sqrt{(1-\gamma)^2 - (1-\gamma)}; \\ \lim_{s\to 1} \lambda_2 &= -1, \quad \lim_{s\to 1} \nu_2 = -\gamma - \sqrt{(1-\gamma)^2 - (1-\gamma)}. \end{aligned}$$

This can be readily seen by substituting $s = 1 + \varepsilon$ and $\nu = -1 + \tilde{\nu}\varepsilon + \mathcal{O}(\varepsilon^2)$ into the quintic polynomial (7.1) and solving for $\tilde{\nu}$. We obtain two solutions $\nu_{1/2}$ which we then substitute into the expression for λ. A short calculation then shows that λ is continuous in ε which implies continuity of double roots. ∎

Lemma 7.2. For fixed $s > 0$, $d_s(\lambda, \nu) = 0$ is a cubic polynomial with respect to ν. As $\operatorname{Re}\lambda \to +\infty$, the real parts of two roots, denoted as ν_1 and ν_2, go to $+\infty$, while the real part of the third root, denoted as ν_3, goes to $-\infty$.

Proof. For $|\lambda| \to \infty$, one readily notices that $|\nu| \to \infty$ for solutions of $d_s = 0$. Poincaré inversion therefore gives all solutions using the Newton polygon for the inverted equation, that is, solving

$$[1-(1-2\gamma)\varepsilon]\delta^3 + [-2s\varepsilon - (1-2\gamma)s\varepsilon^2]\delta^2 + [-\varepsilon + (1-\gamma+s^2)\varepsilon^2]\delta + s\varepsilon^2 = 0,$$

where $\varepsilon = 1/\lambda$ and $\nu = 1/\delta$. We find three roots with

$$\begin{aligned}\delta_1 &= s\varepsilon + \mathcal{O}(\varepsilon^2)\\ \delta_2 &= \varepsilon^{1/2} + \mathcal{O}(\varepsilon)\\ \delta_3 &= -\varepsilon^{1/2} + \mathcal{O}(\varepsilon),\end{aligned}$$

or, in terms of λ and ν,

$$\begin{aligned}\nu_1 &= \frac{\lambda}{s} + \mathcal{O}(1)\\ \nu_2 &= \lambda^{1/2} + \mathcal{O}(1)\\ \nu_3 &= -\lambda^{1/2} + \mathcal{O}(1).\end{aligned}$$

■

Lemma 7.3. The pointwise growth rate is continuous in s.

Proof. By Lemma 7.1, double roots depend continuously on s. We need to show that the pinching condition depends continuously on s. For this, we first remark that the pinching condition is continuous as long as double roots are simple. In that case, the roots depend continuously on s along any compact part of the curve connecting the double root with $\lambda = +\infty$ in the complex plane, so that the maximal real part of roots that satisfy the pinching condition is continuous in s. In general, it is not difficult to see that the pointwise growth rate is upper semi-continuous. Indeed, suppose that the roots $\nu_{1/2}$ are separated from ν_3 in $\operatorname{Re}\lambda \geqslant \eta$. Then the infimum of the distance will be strictly positive and a continuous function of s, which shows that the pointwise growth rate cannot increase under perturbations. To show lower semi-continuity, we need to consider multiple double roots. In our case, there are precisely four possible cases, characterized by the leading order terms in the local Taylor jet:

(i) $d_s(\lambda,\nu) = d_{20}\hat\lambda^2 + d_{11}\hat\lambda\hat\nu + d_{02}\hat\nu^2$,

(ii) $d_s(\lambda,\nu) = d_{10}\hat\lambda + d_{03}\hat\nu^3$,

(iii) $d_s(\lambda,\nu) = d_{20}\hat\lambda^2 + d_{11}\hat\lambda\hat\nu + d_{03}\hat\nu^3$,

(iv) $d_s(\lambda,\nu) = d_{20}\hat\lambda^2 + d_{03}\hat\nu^3$,

where $\hat\nu = \nu - \nu_*$ and $\hat\lambda = \lambda - \lambda_*$, and (λ_*, ν_*) is the degenerate double root. Here, the coefficients $d_{j\ell}$ are assumed to be nonzero. To see that these are the only relevant cases, notice that the coefficients of $\hat\lambda^2$ and $\hat\nu^3$ are nonzero because they are independent of ν_*, λ_*. One then simply enumerates possibilities for vanishing lower-order terms.

In fact, a short explicit calculation shows that case (iii) does not occur in our system for $\gamma \in (0,1)$. In case (i), only two roots $\hat{\nu}$ coalesce near the singularity, so that the pinching condition is either satisfied for all double roots or not.

It remains to show that there are always pinched double roots near the origin in cases (ii) and (iv). In case (ii), one finds precisely two double roots in a neighborhood. Letting $\hat{\lambda} = \varepsilon e^{i\varphi}$, one finds that the roots are permuted cyclically after one loop, which implies that none of the roots possesses a unique analytic continuation. The same argument shows that there exist pinched double roots near $\hat{\lambda} = 0$ in case (iv). ∎

Lemma 7.4. For $s \gg 1$, the pointwise growth rate is negative, that is, $\operatorname{Re}\lambda < 0$ for the first pinched double root.

Proof. It is sufficient to show that for sufficiently large $s \gg 1$, roots $\nu(\lambda)$ to $d_s(\lambda,\nu) = 0$ do not have $\operatorname{Re}\nu = -1$ as long as $\operatorname{Re}\lambda \geqslant 0$. This would imply that the roots $\nu_{1/2}$ that converge to $+\infty$ according to Lemma 7.2 are separated from the root ν_3 that converges to $-\infty$ as $\operatorname{Re}\lambda \to \infty$. Substituting $\operatorname{Re}\nu = -1$ into $d_s(\lambda,\nu) = 0$ gives

$$0 = -A(\operatorname{Im}\nu)^6 - (5A^2 + 4A + B)(\operatorname{Im}\nu)^4 - (8A^3 + 4A^2 + 4AB)(\operatorname{Im}\nu)^2 - (4A^4 + 4A^2B) > 0,$$

where $A = \operatorname{Re}\lambda + s - (1-\gamma) > 0$ and $B = (1-\gamma) - (1-\gamma)^2 > 0$. ∎

Lemma 7.5. For $s > 0$, $s \ll 1$, the pointwise growth rate is positive.

Proof. We can find double roots explicitly for $s = 0$ and expand in s, using the quintic polynomial (7.1). The leading-order terms are

$$\begin{aligned}
\nu_1 &= \tfrac{1-2\gamma}{2\gamma} s & \lambda_1 &= 1 - 2\gamma \\
\nu_2 &= -\tfrac{1-2\gamma}{2(1-\gamma)} s & \lambda_2 &= 0 \\
\nu_3 &= (2\gamma - 2\gamma^2)^{\frac{1}{3}} s^{-\frac{1}{3}} & \lambda_3 &= (1-\gamma) + \tfrac{1}{2}(2\gamma - 2\gamma^2)^{\frac{1}{3}} s^{\frac{2}{3}} \\
\nu_4 &= (2\gamma - 2\gamma^2)^{\frac{1}{3}} e^{\frac{2\pi \mathrm{i}}{3}} s^{-\frac{1}{3}} & \lambda_4 &= (1-\gamma) + \tfrac{1}{2}(2\gamma - 2\gamma^2)^{\frac{1}{3}} e^{\frac{2\pi i}{3}} s^{\frac{2}{3}} \\
\nu_5 &= (2\gamma - 2\gamma^2)^{\frac{1}{3}} e^{\frac{4\pi \mathrm{i}}{3}} s^{-\frac{1}{3}} & \lambda_5 &= (1-\gamma) + \tfrac{1}{2}(2\gamma - 2\gamma^2)^{\frac{1}{3}} e^{\frac{4\pi \mathrm{i}}{3}} s^{\frac{2}{3}}
\end{aligned}$$

On the other hand, we find roots ν of $d_s(\lambda,\nu) = 0$ with $\operatorname{Re}\nu = 0$ only for values of λ in the essential spectrum, where

$$\lambda_\pm = \mathrm{i}sk^2 + \frac{1 - 2\gamma - k^2}{2} \pm \sqrt{\frac{(1-2\gamma-k^2)^2}{4} + (1-\gamma)k^2}. \tag{7.2}$$

Noting that $\operatorname{Re}\lambda_+'(k^2) \geqslant 0$ and $\lim_{|k|\to+\infty} \widetilde{\lambda}_+ = 1-\gamma$, we have $\sup_{k\in\mathbb{R}} \widetilde{\lambda}_+(k^2) = 1-\gamma$.

Now consider the right-most double root (λ_3, ν_3). We examine the pinching condition on a curve $\operatorname{Re}\lambda \to +\infty$. Since $\operatorname{Re}\lambda_3 > 1-\gamma$, $\operatorname{Re}\nu_j \neq 0$ on this curve. On the other hand, $\operatorname{Re}\nu_3 > 0$, so that this double root cannot satisfy the pinching condition.

Next, consider the complex conjugate double roots $(\lambda_{4/5}, \nu_{4/5})$. This time, $\operatorname{Re}\nu_{4/5} < 0$, so that, by Lemma 7.2, the double root lies to the left of $\lambda_+(k^2)$, but to the right of $\lambda_-(k^2)$. This implies that there is one and only one root ν crossing the imaginary axis on a curve from the double root $\lambda_{4/5}$ to $\operatorname{Re}\lambda = +\infty$. This shows that these double roots satisfy the pinching condition. ∎

Lemma 7.6. For $s > 0$, suppose that $(\mathrm{i}\omega, \nu)$ is a double root of the dispersion relation that satisfies the pinching condition. Then $\omega \neq 0$.

Proof. We can substitute $\lambda = 0$ in the equation for double roots and find a cubic polynomial in ν,

$$d_s(0, \nu) = s^2\nu^2 + s(1 - 2\gamma + \nu^2)\nu + (1 - \gamma)\nu^2.$$

One readily verifies that this polynomial does not have double roots when $\gamma \neq 1/2$. For $\gamma = 1/2$, the double root is given by $\nu = 0$, with the third root located at $-(1 + 2s^2)/2 < 0$. Since there are no crossings $\nu \in \mathrm{i}\mathbb{R}$ for $\lambda > 0$ (7.2), and since for $\lambda \to \infty$ we have two roots with $\operatorname{Re}\nu \to +\infty$, we can conclude that the two roots that collide in the double root have $\operatorname{Re}\nu > 0$ for all $\lambda > 0$ and hence do not satisfy the pinching condition. ■

§ 7.2. Uniqueness of complex double roots

Lemma 7.7. There are at least three real double roots, counted with multiplicity.

Proof. We need to show that the quintic polynomial (7.1),

$$q(\nu, s) = -2s\nu^5 - s^2\nu^4 + 4s\nu^3 + [4\gamma(1 - \gamma) + 2s^2]\nu^2 - 2(1 - 2\gamma)^2 s\nu - (1 - 2\gamma)^2 s^2,$$

possesses at least three real roots. For this, one verifies that $q(0, s) < 0$, $q(1, s) > 0$, and $q(-s/2, s) > 0$ for all $s > 0$ and all $\gamma \in (0, 1)$. This implies the existence of three roots $\nu_1 \in (-s/2, 0)$, $\nu_2 \in (0, 1)$, and $\nu_3 \in (1, \infty)$. ■

References

[1] J. Boissonade, E. Dulos and P. De Kepper. Turing patterns: from myth to reality. In "Chemical waves and patterns", R. Kapral, K. Showalter (eds.), Kluwer, Dordrecht, (1995) 221–268.

[2] L. Brevdo and T.J. Bridges. Absolute and convective instabilities of spatially periodic flows. *Phil. Trans. R. Soc. London A* **354** (1996), 1027–1064.

[3] R.J. Briggs. *Electron-stream interaction with plasmas.* MIT Press, Cambridge, 1964.

[4] V. Castets, E. Dulos, J. Boissonade and P. De Kepper. *Experimental evidence of a sustained standing Turing-type nonequilibrium chemical pattern. Phys. Rev. Lett.* **64**, 2953–2956.

[5] G. Dee and J. S. Langer. *Propagating pattern selection.* Phys. Rev. Lett. **50** (1983), 383–386.

[6] A.N. Bers. *Space–time evolution of plasma instabilities–absolute and convective.* In: M.N. Rosenbluth, R.Z. Sagdeev (Eds.), Handbook of Plasma Physics, North-Holland, Amsterdam, 1983.

[7] R. Goh, S. Mesuro, and A. Scheel. *Coherent structures in reaction-diffusion models for precipitation.* In *Precipitation patterns in reaction-diffusion systems*, Research Signpost, 2010, 73–93.

[8] R. Goh, S. Mesuro, and A. Scheel. *Spatial wavenumber selection in recurrent precipitation.* SIAM J. Appl. Dyn. Sys. *10* (2011), 360–402.

[9] R.E. Liesegang. *Über einige Eigenschaften von Gallerten.* Naturwissenschaftliche Wochenschrift **11**, Nr. 30, (1896) 353–362.

[10] A. Lunardi. *Analytic Semigroups and Optimal Regularity in Parabolic Problems.* Birkhäuser, Boston (1995).

[11] J. Maddocks. *Restricted quadratic forms and their application to bifurcation and stability in constrained variational principles.* SIAM J. Math. Anal. **16** (1985), 47–68.

[12] Y. Morita and T. Ogawa. *Stability and bifurcation of nonconstant solutions to a reaction-tdiffusion system with conservation of mass.* Nonlinearity **23** (2010), 1387–1411.

[13] A. Pogan and A. Scheel. *Instability of Spikes in the Presence of Conservation Laws.* Z. Angew. Math. Phys. **61** (2010), 979–998.

[14] J.D.M. Rademacher, B. Sandstede, and A. Scheel. *Computing absolute and essential spectra using continuation.* Physica D **229** (2007), 166–183.

[15] B. Sandstede and A. Scheel. *Period-doubling of spiral waves and defects.* SIAM J. Appl. Dyn. Syst. **6** (2007), 494–547.

[16] B. Sandstede and A. Scheel. *Absolute and convective instabilities of waves on unbounded and large bounded domains.* Physica D **145** (2000), 233–277.
[17] A. Scheel. *Spinodal decomposition fronts in the Cahn-Hilliard equation.* Preprint.
[18] A. Turing. *The chemical basis of morphogenesis.* Phil. Trans. Roy. Soc. B **237** (1952), 37–72.
[19] W. Van Saarloos. *Front propagation into unstable states* Phys. Rep. **386** (2003), 29-222.